

AD-754 427

DOSIMETRIC CHARACTERISTICS OF HZE
PARTICLES IN SPACE

Hermann J. Schaefer

Naval Aerospace Medical Research Laboratory

Prepared for:

National Aeronautics and Space Administration

15 November 1972

DISTRIBUTED BY:

NTIS

National Technical Information Service
U. S. DEPARTMENT OF COMMERCE
5285 Port Royal Road, Springfield Va. 22151

Reproduced by
**NATIONAL TECHNICAL
INFORMATION SERVICE**
U.S. Department of Commerce
Springfield, VA 22151

5

Unclassified

Security Classification

DOCUMENT CONTROL DATA - R & D

Security Classification of title, body of abstract and indexing annotation must be entered when the overall report is classified

1. ORIGINATING ACTIVITY (Corporate author) Naval Aerospace Medical Research Laboratory Pensacola, Florida 32512		2a. REPORT SECURITY CLASSIFICATION Unclassified	
		2b. GROUP N/A	
3. REPORT TITLE DOSIMETRIC CHARACTERISTICS OF HZE PARTICLES IN SPACE.			
4. DESCRIPTIVE NOTES (Type of report and inclusive dates) N/A			
5. AUTHOR(S) (First name, middle initial, last name) Hermann J. Schaefer			
6. REPORT DATE 15 November 1972		7a. TOTAL NO. OF PAGES 30	7b. NO. OF REFS 18
8a. CONTRACT OR GRANTING NASA W-13, 280		9a. ORIGINATOR'S REPORT NUMBER(S) NAMRL 1172	
b. PROJECT NO.		9b. OTHER REPORT NO(S) (Any other numbers that may be assigned this report) No. 47	
c.			
d.			
10. DISTRIBUTION STATEMENT Approved for public release; distribution unlimited.			
11. SUPPLEMENTARY NOTES Prepared for the National Aeronautics and Space Administration		12. SPONSORING MILITARY ACTIVITY	
13. ABSTRACT HZE particles, i.e., galactic heavy primaries with very high values of Linear Energy Transfer (LET) pose a special radiation hazard on manned space missions. While cellular destruction by single hits has been demonstrated, more general data on dose/effect relationships are not available since conventional concepts and units of radiation dosimetry are not applicable. The report summarizes existing knowledge on the energy spectrum of galactic heavy primaries and analyzes the microdosimetric pattern of energy dissipation in tissue. It is shown that the LET distribution shows a steep negative slope with the frequency of events decreasing steeply with increasing LET down to less than one event per cm ³ tissue per day at 4000 kev/micron tissue. Assessing the HZE particle hazard requires new approaches in both radiobiological experimentation and dosimetric instrumentation.			

19

DD FORM 1473

1 NOV 65

(PAGE 1)

Unclassified

Security Classification

SN 0101-807-6801

Unclassified

Security Classification

14 KEY WORDS	LINK A		LINK B		LINK C	
	ROLE	WT	ROLE	WT	ROLE	WT
Space radiation dosimetry HZE particles, Radiation hazards from HZE particles, Microdosimetry of						

ib

Unclassified

Security Classification

Approved for public release; distribution unlimited.

DOSIMETRIC CHARACTERISTICS OF HZE PARTICLES IN SPACE

Hermann J. Schaefer

NASA Order No. W-13,280

Approved by

Ashton Graybiel, M.D.
Assistant for Scientific Programs

Released by

Captain N. W. Allebach, MC USN
Officer in Charge

15 November 1972

NAVAL AEROSPACE MEDICAL RESEARCH LABORATORY
NAVAL AEROSPACE MEDICAL INSTITUTE
NAVAL AEROSPACE AND REGIONAL MEDICAL CENTER
PENSACOLA, FLORIDA 32512

SUMMARY PAGE

THE PROBLEM

The name HZE Particles has become customary for the small fraction of galactic heavy primaries with Linear Energy Transfer (LET) values substantially larger than those of conventional nuclear radiations. HZE particles represent a component of ionizing radiation in space that is essentially unexplored as to its biological significance. Although cellular destruction by single hits has been demonstrated in pilot experiments, broader information on dose/effect relationships is missing. General agreement seems to exist merely on the negative proposition that conventional dosimetric concepts and units are not applicable. Eye flashes experienced by the astronauts on lunar missions, presumably triggered by HZE particles, have deepened concern lest microlesions from HZE particles might pose a subtle yet insidious hazard especially for non-proliferating cell systems in the human body, such as the CNS.

The composition of the primary spectrum of HZE particles in space as well as the physical characteristics of their interaction with matter are well understood. However, the pertinent information reported by physicists usually is presented in terms not directly suitable for dosimetric interpretation. This report attempts to present the basic data on the physics of HZE particles with special consideration of the needs of the experimenter planning to study effects on biological systems.

FINDINGS

Discrepancies between energy spectra of galactic heavy primaries reported by various investigators require establishing a compromise model before flux densities and hit frequencies in special targets are analyzed. For better descriptiveness, the model is converted to the range spectrum which allows direct reading of flux densities for varying shield thickness or target depth. The iron group ($Z = 24$ to 28) as the heaviest component of the HZE particle spectrum is selected for detailed analysis. It is shown that the LET distribution shows a steep negative slope with hit frequencies dropping to less than one hit of maximum LET per cc tissue per 24 hours. As an alternate way of presentation, the LET distribution is also established in terms of integral track length which furnishes a more complete picture of the energy dissipation pattern in tissue. The problems posed by the peculiar LET distribution of HZE particle irradiation for the design of both radiobiological experimentation and dosimetric instrumentation are pointed out.

INTRODUCTION

Heavy nuclear particles as a component of primary cosmic radiation or, as it is preferably called now, galactic radiation, were discovered rather late in the history of cosmic ray research. Although the interpretation of galactic radiation as an extremely hard gamma radiation was abandoned early in favor of nuclear particles, protons were considered for a long time the only constituent. The exclusion of any other particles from consideration was largely due to the influence of cosmological theory which held that the interstellar medium was hydrogen. It therefore was much against expectation and under the skeptical smile of many of their colleagues when a joint team of the Universities of Minnesota and Rochester under E. P. Ney (1) undertook in summer 1948 to expose a stack of nuclear emulsions in a skyhook balloon to the primary galactic radiation. A remarkable payload was recovered on that historical flight. The emulsions of the first and three consecutive flights contained a total of 300 tracks defying any classification in terms of the types of ionizing particles known at that time. Some of the tracks consisted of solid silver ribbons several microns thick indicating that particles with truly enormous ionizing powers had penetrated the emulsion. Ney and his teammates interpreted their findings correctly at first sight: they had discovered the heavy nuclei of the primary galactic radiation.

Soon after the discovery radiobiologists realized that heavy nuclei represented an entirely new kind of ionizing radiation also in their domain with a mode of action on living matter entirely different from natural and artificial radiations of terrestrial origin (2). At about the same time Zirkle and Bloom (3) experimented with artificial microbeams of protons attempting to bombard different parts of individual cells. Although the direct relevance of their work to the problem of galactic heavy particles was quite obvious, the avenue of a joint research effort that presented itself so clearly was never entered.

Direct experimental evidence of the microbeam effectiveness of heavy particles was presented by Chase (4) who demonstrated, in balloon-borne animal experimentation, that single traversals of HZE particles led to complete destruction of the melanoblasts, the pigment-producing cells, in the hair follicle of the black mouse. Other experimenters demonstrated cellular destruction from single hits of heavy nuclei for other specimens such as artemia salina eggs (5) and maize embryos (6).

Except for the just mentioned and a few other sporadic pilot experiments concerning radiobiological aspects, studies with heavy primaries all through the fifties were conducted exclusively by astrophysicists hoping to obtain clues on the origin of galactic radiation and other cosmological problems. Of special importance in this respect was the question whether the atomic composition of the heavy spectrum reflected the abundances of chemical elements in the universe as they followed from analyses of meteorites and spectroscopic data in astronomy. The highest Z number commonly found in heavy nuclei recordings is that of iron, $Z = 26$. Heavier nuclei have been reported only occasionally as individual events. Not until 1967 was this problem attacked in a

more systematic way by P. H. Fowler (7) who flew very large emulsions sheets in balloons at low latitudes where the high geomagnetic cutoff excluded all nuclei of lower energies thereby preventing possible misinterpretation of Z numbers. Fowler's emulsions demonstrated indeed that the entire Periodic System up to uranium is represented in the primary galactic radiation. In fact, the appearance of some tracks of superheavies strongly suggests that they were produced by nuclei heavier than uranium. While these findings are quite exciting for astrophysicists they do not pose a serious problem from the standpoint of radiation safety in space because of the extremely low frequency of superheavy nuclei. Their relative abundance as compared to the iron group ($Z = 24 - 28$) is of the order of 10^{-4} . That means that for critical target areas in the human body, such as the retina or other parts of the CNS where a comparatively small number of irreplaceable cells carry essential functions, the hit probability is extremely small.

In 1957 man-made heavy nuclei became available for the first time from the Heavy Ion Linear Accelerator (HILAC) in the Lawrence Radiation Laboratory at Berkeley, later joined by a similar machine at Yale University. To be sure, artificial ion beams from the HILAC are severely limited in regard to attainable Z numbers and energies. Their very small penetrating powers restrict biological experimentation to monocellular specimens such as phages and viruses. Nevertheless, the HILAC opened a whole new era of most fruitful studies in cellular radiobiology (8) greatly clarifying the basic concepts of the Target Theory and demonstrating that, for heavy particles, single hits retain their unique destructiveness down to the lowest dose levels. Only very recently was the severe energy limitation of the HILAC overcome by using the cyclotron principle and accelerating nitrogen ions to 36 Gev in the Bevatron. Tobias and collaborators (9) promptly tried and succeeded in producing the eye flash phenomenon with these ions. While this progress removes the restrictions with regard to penetrating power, the ultimate goal of long-term total body irradiation of mammals at low dose rates with man-made heavy particles remains still out of reach.

Proving that the old tenet of seeing is believing still seems to hold for scientists and non-scientists alike, an abrupt change of the climate of opinion occurred when the astronauts of the lunar missions reported the eye flash phenomenon predicted as early as 1952 by Tobias (10). Suddenly serious concern was voiced by many lest the microlesions from heavy particles might constitute a subtle yet insidious long-term radiation hazard of a unique nature to the astronauts. In these recent discussions, the term HZE particle is customarily used to set apart heavy primaries with exceptionally high linear energy transfer (LET) from the heavy component of the primary radiation in general.

Perhaps the most striking evidence for the unique destructiveness of HZE particles is their ability to produce, with single hits, microlesions in practically any insulating organic or inorganic solid material with certain plastics being most sensitive. Even without magnifying or developing techniques the lesions are directly visible in the electron microscope. Magnified by etching in sodium hydroxide or other strongly attacking solutions, the lesions become visible under the light microscope. As Fleischer

and collaborators pointed out (11), the ability of an ionizing particle to produce an etchable lesion depends on its LET with the critical LET threshold varying widely for different solids. Since the microlesions are not at all affected even by very large doses of ionizing radiation of low LET, plastic detectors are singularly qualified as sensors for HZE particles on space missions of long duration. A certain drawback is their low sensitivity limiting them to the extreme upper end of the LET spectrum of HZE particles. On the other hand, this limitation might actually prove an advantage making plastic foils the choice as dosimeters for the particular fraction of the HZE particle flux that is not amenable to a quantitative assessment in terms of ordinary dosimetric units. Using aligned triplets of plastic foils, Benton (12) designed a technique for combined Z and LET resolution taking into consideration the particular configuration of the heavy galactic spectrum in deep space outside the magnetosphere.

Projecting the foregoing brief review into the future, one feels inclined to voice a word of caution. Doubtless, the peculiar hazard from HZE particles to man in space finally is, 24 years after the discovery, recognized in its true proportions. However, the rule that once scientists have learned to ask the right question the answer is right around the corner might not hold in this case. At stake is the assessment of subtle long-term damage from chronic exposure to an essentially new kind of ionizing radiation. Extended exposures of test animals at low dose rates would appear the only way to conclusive data. The task of providing such exposures in space-borne experimentation as well as in the accelerator laboratory is beset with formidable difficulties. The ultimate answer therefore may still lie in a more distant future.

In planning radiobiological experiments with HZE particles, an obvious prerequisite is detailed information on the physical characteristics of heavy particle interaction with matter. Although the phenomena involved are well understood, physicists do not always present the results in terms that lend themselves easily to dosimetric interpretation. It is the purpose of this treatise to give a concise self-sustained review of the basic characteristics of galactic heavy primaries in general and of HZE particles in particular with particular emphasis on radiobiological interpretation. We propose to do so in two steps. We shall analyze first the basic properties of heavy particles as such and their interaction with matter. Secondly, we shall combine the findings with the actual make-up of galactic radiation in space and establish hit frequencies in tissue for the various types of HZE particles.

BASIC TERMS AND RELATIONSHIPS

Although there is general agreement among radiobiologists that the conventional dosimetric system using the mean absorbed energy per-unit volume of tissue for quantitating dose is not applicable to HZE particles, satisfactory alternate systems or units have not been established so far since the mode of action of HZE particle irradiation on living matter is poorly understood. The magnitude lying at the root of the problem is Linear Energy Transfer (LET). It denotes the rate of energy dissipation along the path of a charged particle traveling through tissue. In radiobiology and health physics, LET is measured in kilo-electron volts per micron tissue (kev/micron T).

In physics and nuclear engineering the term dE/dx is used instead of LET and the preferred unit is million electron volts per gram per cm^2 of matter ($\text{Mev}/(\text{g}/\text{cm}^2)$). 1 kev/micron T equals 10 $\text{Mev}/(\text{g}/\text{cm}^2)$ if density 1.0 is assumed for tissue. In a given material such as tissue the LET of a charged particle depends directly on the square of its charge and inversely, obeying a more complex function, on its speed or kinetic energy. Since a heavy nucleus of Atomic Number Z and Atomic Weight A carries Z times the charge and, at the same speed, A times the kinetic energy of a proton, the various functions linking range, energy, and LET of a heavy nucleus can be derived from the corresponding functions for protons by multiplication or division by the factors Z^2/A or Z^2 or Z respectively. A further simplification is achieved if kinetic energy is not expressed simply in kev or Mev of the entire nucleus, but in terms of the kinetic energy per atomic mass unit (amu) of the nucleus where the Atomic Weight A determines the number of amu's. The kinetic energy per amu often is called energy per nucleon (kev/nucleon or Mev/nucleon). This usage stems from the term nucleon for amu.

An example might explain the just outlined relations. Iron has the Atomic Number $Z = 26$ and the Atomic Weight $A = 56$. That means an iron nucleus of the primary galactic radiation has $Z^2 = 676$ times the LET and 56 times the kinetic energy of a proton of the same speed. Yet its kinetic energy expressed in Mev/nucleon is the same as that of the proton. It is seen by inspection that the iron nucleus, having $A = 56$ times the kinetic energy of the proton, yet spending that energy $Z^2 = 676$ times faster per unit distance traveled in tissue, must have an $A/Z^2 = 0.083$ times shorter range than the proton. In other words, one can read the range of the iron nucleus from a graph or table showing the range/energy function for protons simply by multiplying the proton range by A/Z^2 . Obviously, this method enormously simplifies storage and presentation of basic data on heavy nuclei. The classic form of that way of presentation is the so-called Rossi graph (13). In its original design even LET is normalized by expressing it in multiples of the minimum LET through which particles of any Z pass at $\beta = 0.97$, i.e., at 97 per cent of the speed of light.

It should be mentioned that the applicability of normalized range/energy and LET/energy relationships to all Z species does not hold rigorously for the very end of the track of a heavy particle where the LET passes through a steep maximum, the so-called Bragg peak. As incident radiation, HZE particles are stripped of all orbital electrons. When slowed down sufficiently in absorbing material they start building up the system of orbital electrons. The capture of electrons leads to a reduction of the effective net charge determining LET as compared to the nominal charge Z . For such a nucleus the LET is no longer Z^2 times larger than that of a proton of equal speed. On the one hand, this effect produces a very substantial decrease of the LET maximum in the Bragg peak. On the other hand, it prolongs the residual range only very moderately because the effective Z becomes anomalous not until the last 50 to 200 microns in tissue have been reached depending on the type of nucleus. The correction of residual range therefore can be safely disregarded in assessments of shielding effects involving macroscopic dimensions of the vehicle frame or heavy equipment or the depth of penetration into the human body. However, the effect has to be considered if the LET distribution in the

microstructure of tissue is to be analyzed in the anomalous region at the end of a particle track in and about the Bragg peak.

Although the Rossi graph or similar unified presentations make for utmost conciseness, their utilization in assessments of hit frequencies from various Z species for specific experimental systems and shield distributions presupposes a certain familiarity with the basic nuclear physics involved. Furthermore, as was just pointed out, they are not applicable if the LET distribution along the individual track in the vicinity of the Bragg peak is to be analyzed. Since the structure and distribution of Bragg peaks in the microstructure of tissue would seem of special interest in the context of the present report, it was felt that the method of normalized presentation should not be used. Data display can still be kept within reasonable limits if it is explicitly done only for selected Z numbers. This approach is all the more advisable inasmuch as presentation of flux densities for heavy particles customarily is done for group representatives rather than for individual Z numbers.

The term "high LET radiation" is often loosely used with different meanings in different contexts. Officially, it is defined by the International Commission on Radiobiological Protection (14) as a radiation with a LET of 3.5 keV/micron T or higher. At 3.5 keV/micron T the QF begins to increase above 1.0 growing continuously until it reaches 20 at 175 keV/micron T. For still higher LET values the definition of appropriate QF's remains an open question. The ICRP expressly states that for radiations with very high LET the concept of dose as energy absorbed per unit volume of tissue breaks down and the units of rad and rem cannot be applied.

THE BRAGG CURVE

From the foregoing explanation, it is seen that setting apart the HZE fraction of the total heavy flux requires identification of the fraction carrying very high LET values. We begin this task with analyzing the LET distribution along the tracks of HZE particles of selected Z numbers in tissue. The classic format in which this function has been presented first is the so-called Bragg curve. It shows LET as a function of residual range. We select Neon ($Z = 10$, $A = 20$) and Iron ($Z = 26$, $A = 56$) as representatives bracketing what is usually considered the relevant Z region for HZE particles. Figures 1 and 2 show the Bragg curves of these two types of particles in tissue. The two plots demonstrate well the complexity of the task of dosimetric classification of high HZE particles. Considering the two particle tracks as microbeams, we see that the local energy deposited in individual cells along the path of a nucleus in tissue varies continuously and considerably almost from cell to cell. For neon nuclei, the LET changes from 194 keV/micron T at a residual range of 1600 microns to 1450 keV/micron T in the Bragg peak at 20 microns. For iron nuclei, the corresponding change extends from 905 keV/micron T at 1600 microns to 4180 keV/micron T in the Bragg peak at 60 microns residual range. Obviously, individual cellular damage along the particle tracks can be expected to show similarly strong variations. However, critical LET thresholds for specific types of such damage are not known at present. Data on track lengths therefore can be presented only for arbitrarily selected LET values. Figure 3 shows a

family of pertinent curves. Eleven different LET thresholds covering the interval from 250 to 4500 keV/micron T have been selected. The abscissa shows Z numbers from 1 to 30 and the ordinate corresponding track lengths for which a particle of a given Z would maintain a LET above the threshold value. The graph demonstrates well the great variety of events that occur in the microstructure of tissue exposed to HZE particles.

TRACK STRUCTURE

As complex as the picture unfolding in Figure 3 is, it still does not tell the full story. LET alone does not furnish, for HZE particles, a complete description of the energy dissipation in the microstructure of tissue. Tracks of equal LET produced by particles of different Z numbers, hence of different energies, differ with regard to the radial spread of the energy distribution from the center of the track to the periphery. This spread is determined by the so-called maximum transferable energy (MTE) to electrons. A HZE particle transmits the MTE to an electron if a central collision occurs. The MTE depends only on the speed of the projectile nucleus. The Z number merely determines the number of collisions per unit path length. A quantitative analysis of the radial structure is an involved task. Without dwelling on the nuclear physics of nucleon-electron collision, we show in Figure 4 the radial spread for an oxygen nucleus at two different energies corresponding to β values of 0.1 and 0.4 where $\beta = v/c$, i.e., expresses the speed of the nucleus as fraction of the speed of light. It is seen that the local dose drops steeply from an extremely high value in the center of the track toward the periphery. It should be noted that the definition of absorbed dose in rad as energy dissipation per unit volume is applied in Figure 4 differentially as energy dissipation in vanishingly small tissue volumes. The applicability of this concept seems questionable for very small volumes because of the quantum nature of the absorption processes. The issue is further complicated by the fact that a large part of the energy transfer in the innermost core of the track leads to excitation of target atoms rather than to complete ionization. Conceivably, this could alter the quantity of damage per rad in the core. However, this latter problem is not unique for HZE particles. It exists in the same way for proton and alpha tracks in tissue. In fact, for the latter two kinds of nuclear particles, the fraction of the total LET going into excitations is even larger than for HZE particles of the same LET.

For particles with very high Z and E values combined, the secondary electrons may travel over distances larger than the radiosensitive target volumes of cellular structures. It is obvious that in such cases gross LET is not a truly relevant parameter anymore. Instead, a restricted LET considering only individual energy transfers below a certain limit would have to be applied for realistic dosimetric interpretation of data. This problem demonstrates the particular difficulties that arise in the attempt of establishing a meaningful dosimetric unit or system for HZE particles.

ATTENUATION THROUGH NUCLEAR COLLISION

The process of ordinary ionization, which was analyzed in detail in the preceding section, is not the only mechanism of attenuation of HZE particles in matter. A completely different second kind of interaction occurs when a HZE particle collides with the nucleus rather than orbital electrons of an atom of the absorbing material. Such a nuclear collision terminates the path of the heavy particle abruptly. Usually, both projectile and target nucleus completely disintegrate into neutrons, protons, and alpha particles. Less frequently, heavier fragments of the colliding nuclei remain intact and are emitted or continue the path of the projectile nucleus undisturbed. Finally, in collisions of particles of very high energies about and beyond 1 Gev, mesons are produced in addition to nuclear fragments.

A nuclear interaction is a probability event that depends on the collision cross sections of the colliding nuclei. That means it cannot be predicted whether at all or at what particular depth in shield or tissue the individual particle will undergo a collision. Accordingly, attenuation through collision can be described quantitatively only in statistical terms by the mean free path for nuclear collision which denotes the depth in absorbing material at which 63 per cent of the particles have been removed from the incident flux by collisions. Numerical values of collision mean free paths are listed in Table I.

Table I

Mean Free Paths in Water for Nuclear Interaction
of HZE Particles

Element	Z	Mean Free Paths cm or g/cm ² Water
C	6	22
Mg	12	16
Ca	20	12
Fe	26	10

The combined action of the basically different processes of ordinary ionization and nuclear collision leads to rather complex relationships concerning the attenuation of HZE particles in matter. It is seen by inspection that particles of low energies in the incident radiation, which have an ionization range substantially shorter than the collision mean free path, have a high probability of escaping nuclear collision completely and spending their entire kinetic energy in ordinary ionizations. These particles represent the radiobiologically most effective fraction of the total fluence since they reach maximum LET in the Bragg peak shortly before they come to rest. Particles of high and very high energies in the incident beam, on the other hand, with ionization ranges substantially greater than their interaction mean free paths, have a

high probability of being removed from the beam by nuclear collisions before they can reach the Bragg peak. Since the primary galactic radiation in free space is a mixture of different Z species, each one in turn represented with a wide continuum of different energies, the transition occurring during attenuation in shielding layers or the human body is extremely complex and can be analyzed only with exact information on Z abundances and energy spectra.

COMPOSITION OF GALACTIC RADIATION IN SPACE

In the section on Basic Terms and Relationships above, we learned that measuring and expressing particle energy per nucleon rather than per particle allows unified data presentation for all Z species. Accordingly, we present the energy spectra of HZE particles by plotting their flux density over energy per nucleon (MeV/nucleon). Although data reported by different experimenters still show discrepancies, it seems generally agreed that, except for protons, all Z species show the same basic configuration of the energy spectrum. Since the alpha component ($Z = 2$, He⁺) is the most abundant component, its spectrum is most accurately known and generally used as reference.

Two main factors influence flux density of galactic particles in space, the magnetic dipole field of the earth and the interplanetary magnetic field created by solar activity. The former field is of significance only on near-earth orbital missions where it creates a complex continuous change of flux density depending on the geomagnetic coordinates of instantaneous position. The pertinent relationships will be discussed in detail later. Outside the magnetosphere of the earth, the interplanetary field remains as a factor modulating galactic radiation. It does so in anticorrelation to the 11-year cycle of solar activity since a strong interplanetary field prevents galactic particles of lower energies from reaching the inner planets whereas a weak field exerts a smaller screening effect thus creating maximum flux density at solar minimum.

Many experimenters have measured flux densities of galactic particles at various phases of the solar cycle and attempted to establish, either by direct measurements or by inference, the spectra at solar minimum and maximum. The most recent data on the spectrum at solar minimum have been communicated by Meyer (15) and those at solar maximum by Mason (16). While the two spectra seem to agree satisfactorily with earlier measurements in the region of medium and low energies, they show a major discrepancy at high and very high energies. At these energies, theory as well as earlier experimental findings indicate consistently that the two spectra should approach each other and finally coincide in line with the assumption that the interplanetary field does not influence nuclei of very high energy. In selecting the spectra of Meyer and Mason for the following analysis, we have used only their medium and low energy sections where solar modulation is strong. For the high-energy section where solar modulation vanishes, a compromise was established between data by Webber (17) and Balasubrahmanyam and collaborators (18) which appear to furnish a more plausible model.

Figure 5 shows the differential energy spectra of galactic alpha particles at solar minimum and maximum established in the just indicated way. It is seen that both spectra are wide continua extending from very low to extremely high energies beyond 10,000 Mev/nucleon. The graph also demonstrates how solar modulation differs for different energies. At very low energy flux density is seen to be larger by a factor of 7 at solar minimum whereas the curves almost fuse at very high energy. The special radiobiological significance of this variation rests in the fact that the particles of lowest energy carry the highest LET. This relationship is indicated in Figure 5 with the curve "LET" to be read over the same abscissa yet using the righthand ordinate scale. LET is expressed in multiples of the minimum LET which all nuclear particles reach at about 3000 Mev/nucleon. The essential feature is the steep increase of LET toward lower energies in the region where the difference of flux densities between solar maximum and solar minimum is highest. Values of minimum LET for representative Z numbers are listed in column 6 of Table II.

As mentioned above, the alpha spectra of Figure 5 hold also for all higher Z numbers if the flux density scale is adjusted by appropriate abundance factors. Here again, available information still shows discrepancies because precise determination of Z numbers is a difficult task for any recording device, be it nuclear emulsion, plastic foil, a solid state detector, or a pulse ionization chamber. Moreover, particle intensities, especially for higher Z numbers, are quite low limiting statistical significance even for exposure times of many days on deep space missions. Most experimenters alleviate both problems by reporting data for Z groups rather than individual Z numbers. Depending on instrumentation, different systems of Z grouping have been used. In the present context, the system shown in Table II seems an appropriate choice. With the relative abundance of the alpha component set equal to 1.00, absolute flux densities for any other Z group can be easily established from the spectra in Figure 5 by multiplying the left ordinate scale by the abundance factors in column 5 of Table II.

Turning to the influence of the geomagnetic field on particle flux density, we forego a discussion of the rather complex relationships governing the deflection of charged particles in a magnetic dipole field. It might merely be mentioned that the screening effect can be accounted for with satisfactory approximation by using the so-called cutoff energy. It indicates the minimum energy/nucleon which a heavy particle must possess if it is to reach the vicinity of the earth. The cutoff energy depends strongly on the geomagnetic latitude of approach. It is very high for particles traveling in the plane of the geomagnetic equator and zero for particles traveling along the magnetic dipole axis. In Figure 5 cutoff energies for 30, 40, 50 and 60° geomagnetic latitude are indicated. According to the explanation above, these energies separate the spectrum into an allowed and forbidden section. At a given latitude, only particles with energies above the cutoff value will arrive. Applying the relationship to actual near-earth orbits, one has to remember that the magnetic dipole axis and the axis of rotation of the earth are tilted against each other by 11.5°. Therefore, the instantaneous geomagnetic latitude of position for an orbit of given geographic inclination obeys a complex function showing a twofold periodicity, one of a period of

Table II
The Heavy Components of Primary Galactic Radiation

Element	Atomic Number, Z	Group Representative, Element	Relative Abundance	Minimum LET, kev/micron T	Z ² /A
He	2	-	1.00	0.80	1.000
Li - F	3-9	C	0.0633	7.2	3
Ne - Si	10-14	Mg	0.0167	29	6
P - Va	15-23	Ca	0.0267	80	10
Cr - Ni	24-28	Fe	0.0333	135	12

about 90 minutes according to the revolving time for a standard near-earth orbit, and one of 24 hours due to the rotation of the Earth.

While the set of curves in Figure 5 and the data in Table II seem to furnish complete information on the HZE particle components of galactic radiation they do not directly show the penetration of the various Z numbers and energies into a shielding layer or the body. Such data, however, are quite essential if one wants to assess residual flux densities within specific vehicles. The assessments in question can be made much more directly if flux densities are presented in the form of the differential range spectrum. In the same way as the differential energy spectrum (Figure 5) presents flux densities per unit energy interval (1 Mev/nucleon), the differential range spectrum presents flux densities per unit range interval (1 g/cm²). Figure 6 shows the range spectra for the galactic alpha component. The curves are direct conversions of the two energy spectra of Figure 5.

In a similar way as the differential energy spectra in Figure 5, the range spectra in Figure 6 can be utilized to derive the corresponding range spectra for heavier Z components by applying the appropriate conversions. Only this time, the conversions are more involved than in the case of the energy spectrum where merely an abundance factor had to be applied to the ordinate scale. As pointed out above in the section on Basic Terms and Relationships, nuclei of any Z have, at the same speed, the same energy per nucleon. However, nuclei with different Z numbers do not have, at the same speed and energy, the same range. As has been shown above, ranges are shorter by the factor A/Z^2 . Since range is involved in the dimensional units of ordinate and abscissa of Figure 6, both scales require conversion. Flux densities on the ordinate have to be multiplied not only by the abundance factor but also by the factor Z^2/A . Ranges on the abscissa have to be divided by the same factor. Conversion factors for all Z groups are listed in column 7 of Table II. It should be noted that the alpha component (He, Z = 2, A = 4) has the unique property that Z^2/A equals A/Z^2 . The differential range spectrum for the alpha component therefore represents a universal reference spectrum from which range spectra for other Z components can be derived without the Z^2/A factor of the alpha component entering the conversion. It is for the same reason that the ranges of protons and alpha particles of the same speed or energy per nucleon are the same.

The division of the range scale of the alpha component by Z^2/A for establishing the spectra for higher Z numbers substantially reduces the ranges as compared to those of lower Z numbers. This indicates the lower penetrating power of nuclei with higher Z numbers for a given energy per nucleon. As a consequence, residual flux densities of these nuclei more strongly reflect local differences in the shield distribution of vehicle frame and equipment and the astronauts' bodies themselves. Furthermore, since for a given Z number the nuclei of lowest energy, i.e., of lowest penetrating power carry the highest LET, the just indicated greater sensitivity of high Z numbers to shielding is further increased for the biologically most effective fraction of the total particle fluence. We demonstrate this proposition quantitatively for the heaviest component, the iron group (Z = 24 to 28), in Figure 7. The spectra marked "incident"

have been established as described above by multiplying the ordinate values of Figure 6 by $Z^2/A = 676/56 = 12.07$ and by the Fe-group/alpha abundance ratio of 0.0033 whereas the abscissa scale has been divided by Z^2/A , i.e., multiplied by $A/Z^2 = 0.0828$. The strong shift of the spectrum to the left, i.e., to lower ranges as compared to the alpha component, is conspicuous.

It is essential to understand clearly that the differential range spectra for the alpha component in Figure 6 and the corresponding spectra for the iron group in Figure 7 marked "incident" describe the make-up of the radiation before it has interacted with or traveled in any absorbing material. As soon as the radiation penetrates matter, nuclear collision events begin to remove nuclei from the beam. Therefore, the differential flux density read for any range R from the incident spectrum will reach depth R only with a value reduced by the collision loss. Since this loss is a negative exponential function of the depth of penetration, the reduction is initially quite small but grows more and more rapidly toward greater depths. The pair of curves in Figure 7 marked "Reaching Depth R" shows the incident spectra corrected for collision loss. Contrary to the incident spectra, the corrected spectra do not describe the make-up of the radiation at a specific location but denote the number of particles coming to rest at various depths R.

Shortly before a particle comes to rest it reaches maximum LET in the Bragg peak. Therefore, the curves marked "Reaching Depth R" in Figure 7 bear special radiobiological significance since they indicate the events of highest local energy dissipation along the path of the radiation. It is these events that are responsible for the microlesions attributed uniquely to HZE particles. It seems of interest to set these terminating particles, the so-called enders or thindowns, apart from the particles that pass all the way through, which for lack of a better name might be called throughshots. It is obvious that the throughshots comprise all particles with ranges greater than depth R. In other words, the local flux density of throughshots at depth R can be obtained by summing up, i.e., integrating, the differential flux densities in the incident spectrum from R to infinity and correcting the sum (integral) for the collision loss occurring on the way from depth Zero to R. The corresponding integral spectra for the iron group at solar minimum and maximum corrected for collision loss are shown in Figure 8 marked "Throughshots". Also shown in Figure 8, carried over unchanged, are the curves marked "Reaching Depth R" from Figure 7. They have been renamed "Enders" in Figure 8 since the abscissa scale, although essentially unchanged, now represents depth in tissue rather than range.

The ordinate notation in Figure 8 "Enders per cm^3 Tissue or Throughshots resp./ ($\text{m}^2\text{hour ster}$)" requires clarification. It is obvious that the frequency of enders cannot be defined for a two-dimensional target area but only for a three-dimensional target volume whereas for the frequency of throughshots area is the appropriate dimensional unit. Plotting the two frequencies for the purpose of a direct comparison on one ordinate scale, therefore, requires a compromise. In using the ordinate scale in Figure 8 for evaluating frequencies, one should visualize a target area of one square meter traversed by throughshots. For the frequency of enders, that same one square meter represents the surface of a thin sheet of one cubic centimeter total volume, i.e.,

of one micron thickness. Visualized in this way, Figure 8 allows a direct comparison of the frequencies of enders and throughshots. It is seen that the former, the local frequency of enders, is always substantially smaller than that of throughshots. It is also seen that the difference in the frequencies of the two types of events depends on shielding. As can be verified from Figure 8, the ratio of enders to throughshots starts from a value as low as 0.075 at the depth of 0.1 g/cm^2 dropping further to 0.04 at 5 g/cm^2 , 0.03 at 10, and 0.02 at 20 g/cm^2 .

In view of the just demonstrated strong dependence of the enders-to-throughshots ratio on shielding or target depth and in view of the unique importance of enders for the HZE particle hazard, it seems of interest to convert the geomagnetic cutoff energies shown above in Figure 5 to ranges for the iron group in Figure 7. The ranges in question are indicated in Figure 7 for the same latitudes selected in Figure 5. It is seen that for middle and low latitudes the ender frequency drops well below one per cent of the one for throughshots and that, in the same latitude region, the ender frequency is a very strong function of latitude. Comparing, for instance, the inclination of about 30° of all past manned near-earth orbital missions to the 50° inclination of the Skylab orbit and reading the corresponding ender frequencies in Figure 7, one recognizes the basic difference between the two types of missions with regard to the HZE particle hazard.

The fact that, for a given Z species, events of maximum LET account only for a very small fraction of the total flux density is a universal characteristic in radiation fields of HZE particles. It distinguishes irradiation with HZE particles from all other kinds of ionizing radiations. In view of the special significance of the phenomenon we proceed to evaluate concrete numerical data for a specific system. For uniform shielding of 1.5 g/cm^2 , 2π incidence and a target volume of 1 cm^3 tissue, the curves in Figure 8 furnish a frequency of .135 enders and 2.23 throughshots. Of these events, all enders are identical in LET whereas the throughshots cover a wide continuum on the LET scale extending from the minimum of $135 \text{ kev}/\mu\text{T}$ to the onset of the Bragg peak. It is seen, then, that the distinction between enders and throughshots falls short of a complete analysis of the LET distribution since it sorts out selectively only the events of maximum LET.

An often used method of describing the microdosimetric energy dissipation for nuclear particles is the LET/track length distribution. It can be presented as differential or integral distribution. The former shows fractional track lengths for specified LET intervals, the latter cumulative track lengths over LET. In the present context, only LET values exceeding the values of conventional nuclear radiations such as neutrons, protons, or alpha particles are of interest. We therefore select a minimum LET of $400 \text{ kev}/\mu\text{T}$ as an arbitrary limit for the analysis. With the Bragg peak for alpha particles reaching $270 \text{ kev}/\mu\text{T}$ the just selected minimum should indeed confine the presentation strictly to HZE particles.

Figure 9 shows the integral LET/track length distribution for the iron group for conditions of solar minimum and an exposure time of 24 hours. The ordinate is a logarithmic scale of track length per cm^3 tissue along which the LET equals or surpasses the abscissa value. Recognizing that the track length covers three and one-half

logarithmic decades as the LET changes from 400 to 4200 keV/ μ T, we realize the enormous steepness of the distribution. At the same time, the distribution demonstrates the extremely low frequency of events of maximum LET quantitatively: We read in Figure 9 a track length of slightly over 10 microns per cm³ tissue per 24 hours for LET values exceeding 4000 keV/ μ T.

CONCLUSIONS

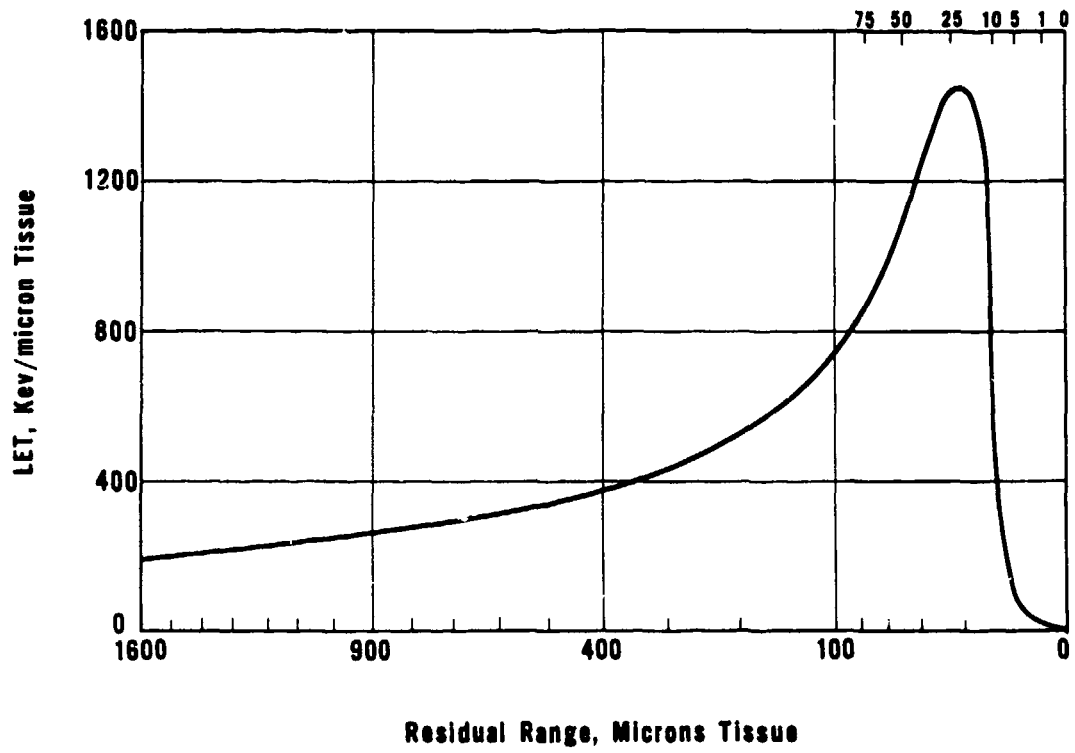
The data in Figures 8 and 9 convey the essential feature of HZE particle exposure in space. It is tantamount to a microbeam irradiation that affects only an extremely small fraction of the total cell population of an exposed target, even for exposure times of weeks. By "extremely small" we mean in this case fractions ranging from 10⁻⁶ to 10⁻⁹ per day depending on the minimum LET one would want to consider. This basic feature presents the radiation pathologist with the question whether the human organism contains organ systems in which destruction of a few cells per day would constitute an above-threshold injury. In addition to the problem of local damage, the question arises what the consequences of long-term total-body exposure on the indicated level would be. A discussion of these issues is outside the scope of this report.

Equally complex is the problem of adequately measuring HZE particle exposure. Resolution of the extremely heterogeneous LET distribution would require very sophisticated pulse discriminating equipment. At the present state of radiobiological knowledge, the instrument designer could not even start to tackle the problem since critical LET thresholds are not known. Furthermore, it seems likely that not only LET as such but also associated coherent track length constitutes a relevant parameter to be measured. These aspects indicate that the HZE particle hazard will have to be accepted, for a number of years to come, as an essentially unknown risk on manned space missions.

REFERENCES

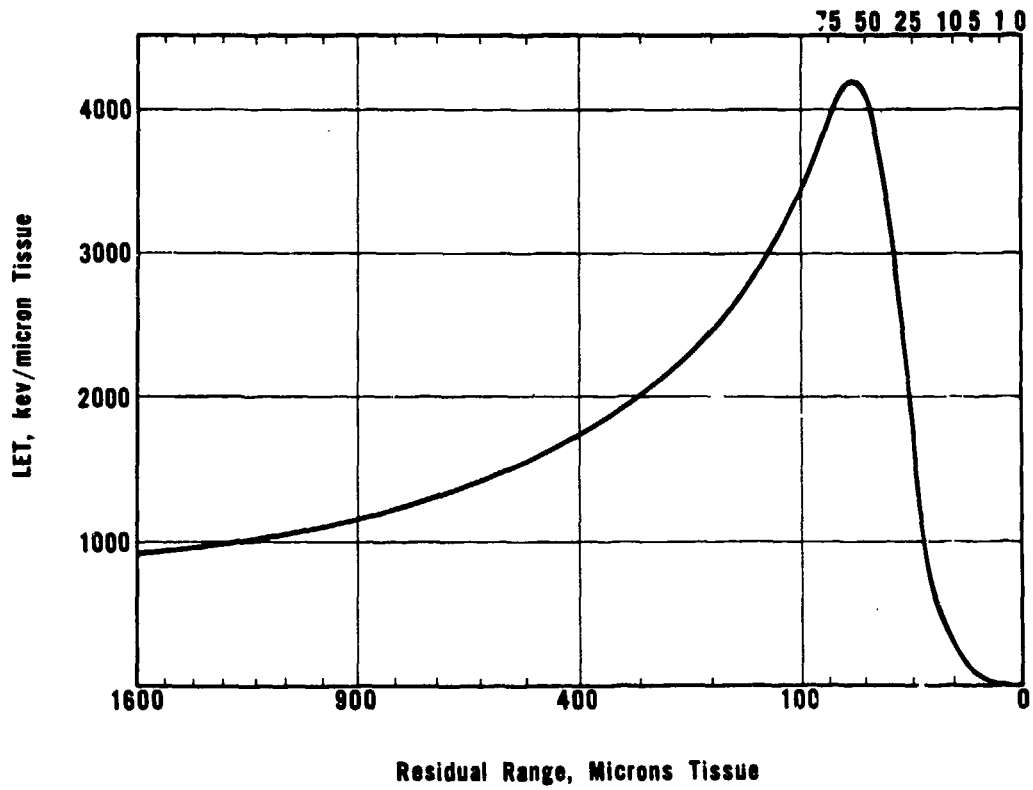
1. Freier, P., Lofgren, E. J., Ney, E. P., Oppenheimer, F., Bradt, H. L., and Peters, B., Evidence for heavy nuclei in the primary cosmic radiation. Phys. Rev., 74: 213-217, 1948.
2. Schaefer, H. J., Evaluation of present day knowledge of cosmic radiation at extreme altitude in terms of the hazard to health. J. Aviat. Med., 21: 375-394, 418, 1950.
3. Zirkle, R. E., and Bloom, W., Irradiation of parts of individual cells. Science, 117: 487-493, 1953.
4. Chase, H. B., Cutaneous effects of primary cosmic radiation. J. Aviat. Med., 25: 388-391, 1954.
5. Eugster, J., Weltraumstrahlung. Bern, Switzerland: Medizinischer Verlag Hans Huber, 1955.
6. Curtis, H. J., Cornseeds affected by heavy cosmic ray particles. Science, 141: 1-2, 1963.
7. Fowler, P. H., Adams, R. A., Cowen, V. G., and Kidd, J. M., The charge spectrum of very heavy cosmic ray nuclei. In: Proceedings of the Royal Society. London. 301: 39-45, 1967.
8. Brustad, T., Molecular and cellular effects of fast charged particles. Rad. Resch. 14: 139-158, 1961.
9. Tobias, C. A., Lyman, J. T., Chatterjee, A., Howard, J., Maccabee, H. D., Raju, M. A., Smith, A. R., Sperinde, J. M., and Welch, G. P., Radiological physics characteristics of the extracted heavy ion beams of the Bevatron. Science, 174: 1131-1134, 1971.
10. Tobias, C. A., Radiation hazards in high altitude aviation. J. Aviat. Med., 23: 345-372, 1952.
11. Fleischer, R. L., Price, P. B., Walker, R. M., Tracks of charged particles in solids. Science, 149: 383-393, 1965.
12. Schaefer, H. J., Benton, E. V., Henke, R. P., and Sullivan, J. J., Nuclear track recordings of the Astronauts' radiation exposure on the first lunar landing mission Apollo XI. Rad. Resch., 49: 245-271, 1972.
13. Rossie, B., High-Energy Particles. New York: Prentice-Hall, Inc., 1952. Pp 35-46.

14. Recommendations of the International Commission on Radiological Protection, ICRP Publication 9. New York: Pergamon Press, 1966.
15. Meyer, P., Cosmic rays in the galaxy. Ann. Rev. of Astronomy and Astrophy. 7: 1-38, 1969.
16. Mason, G. M., Interstellar propagation of galactic cosmic ray nuclei $2 \leq Z \leq 8$ in the energy range 10-1000 Mev per nucleon. J. Astrophy. 171: 139-161, 1972.
17. Webber, W. R., Time variations of low rigidity cosmic rays during the recent sunspot cycle. In: Wilson, J. G., and Wouthuysen, S. A. (Eds.), Progress in Elementary Particle and Cosmic Ray Physics. Vol. VI. New York: John Wiley & Sons, 1962. Pp 75-243.
18. Balasubrahmanyam, V. K., Boldt, E., and Palmeira, R. A. R., Solar modulation of galactic cosmic rays. J. Geophys. Res., 72: 27-36, 1967.



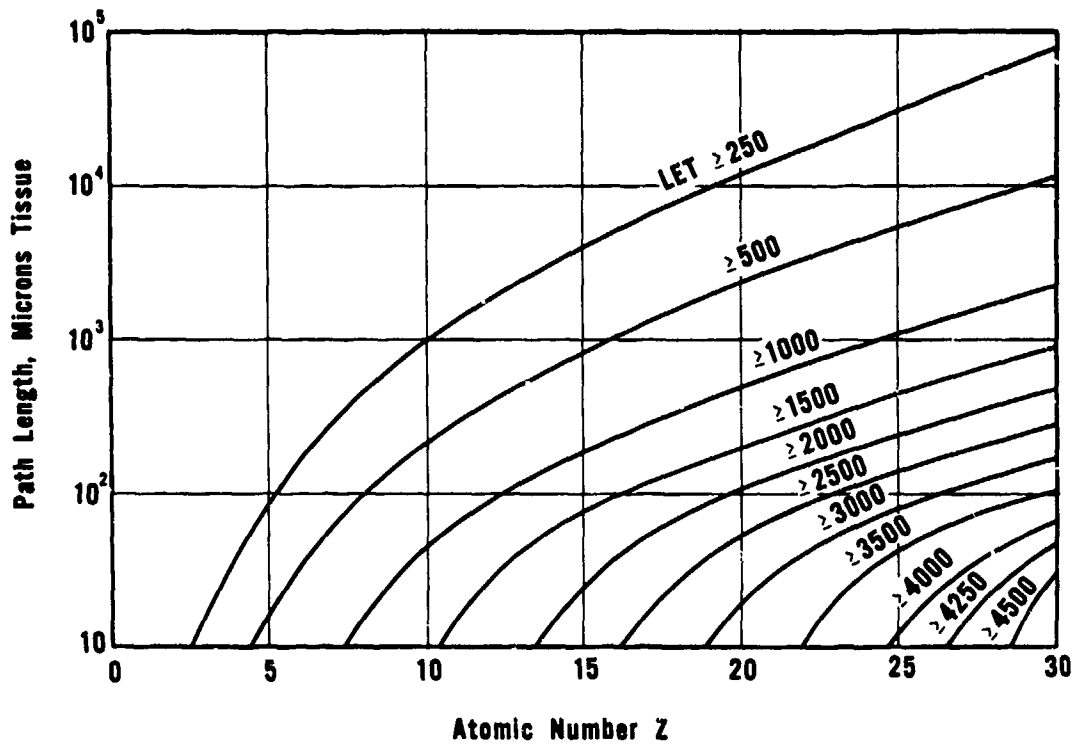
BRAGG CURVE FOR NEON NUCLEI (Z=10, A=20)

FIGURE 1



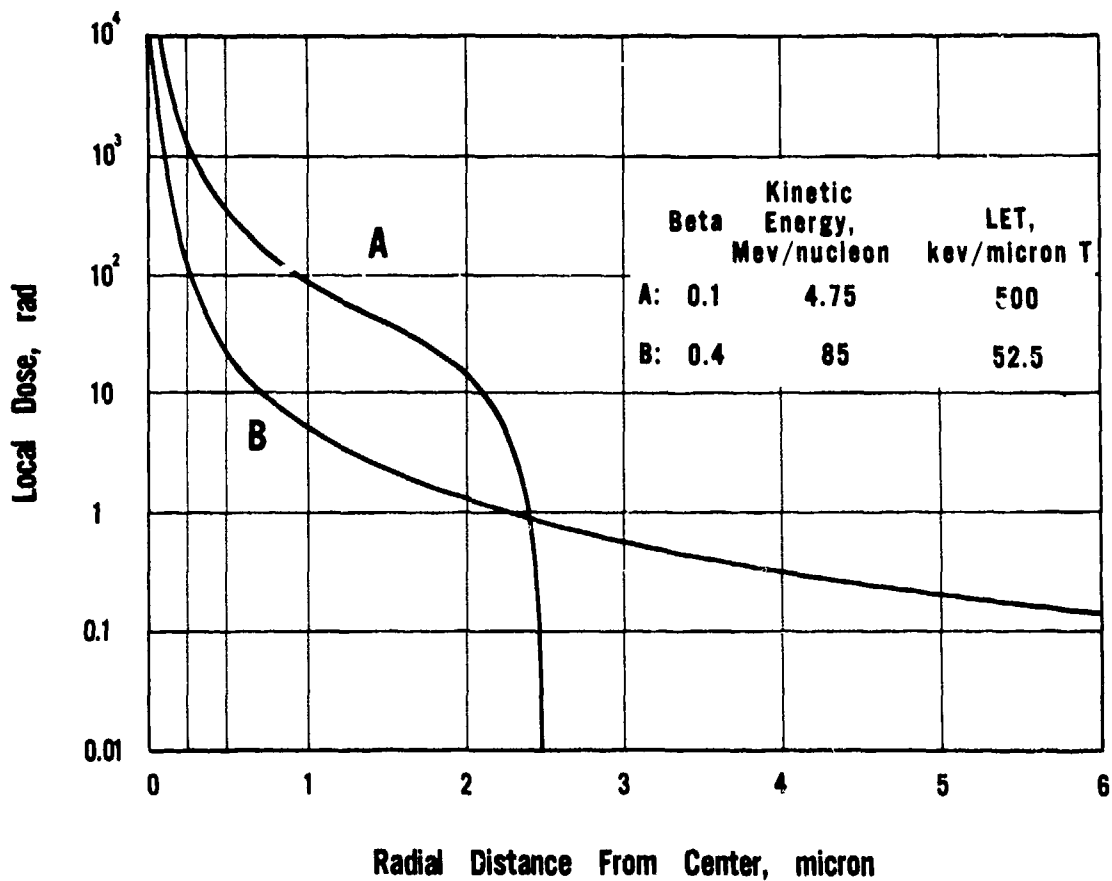
BRAGG CURVE FOR IRON NUCLEI (Z=26, A=56)

FIGURE 2



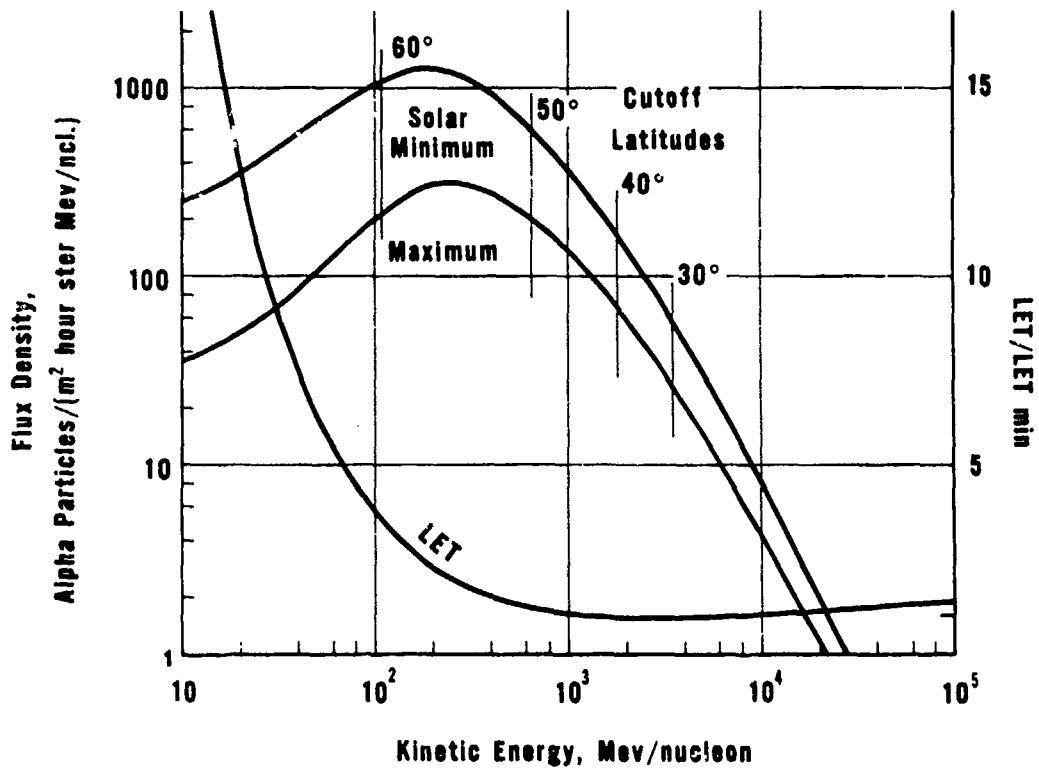
PATH LENGTH OF HZE PARTICLES IN TISSUE FOR VARIOUS LET THRESHOLDS

FIGURE 3



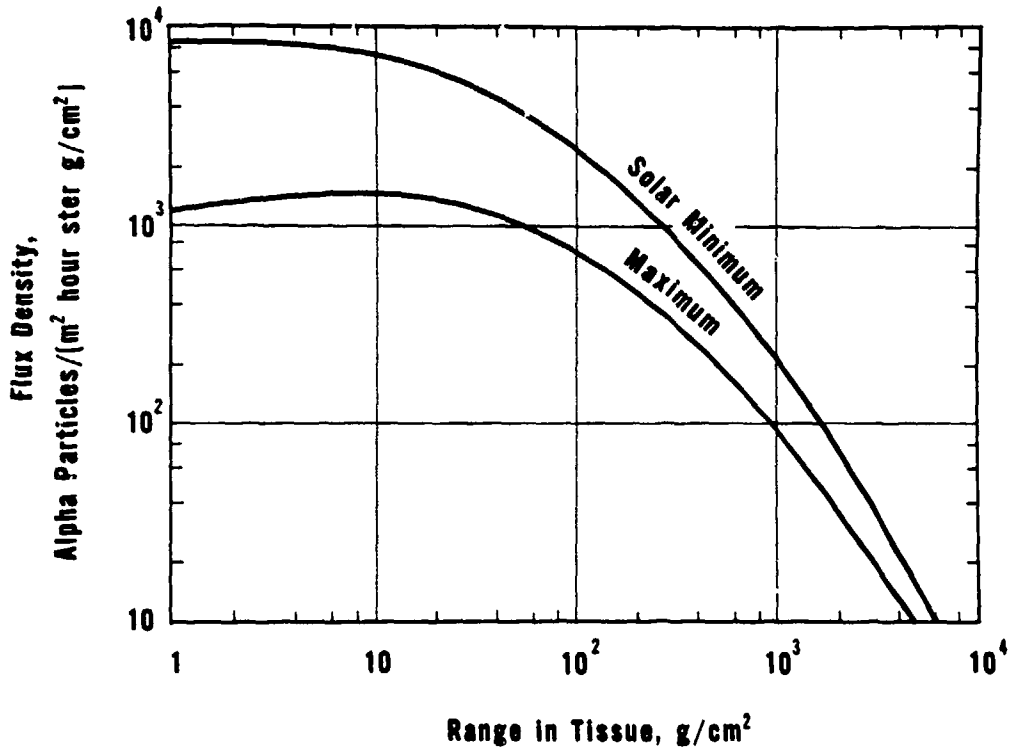
RADIAL SPREAD OF ENERGY DISSIPATION OF OXYGEN TRACK IN TISSUE

FIGURE 4



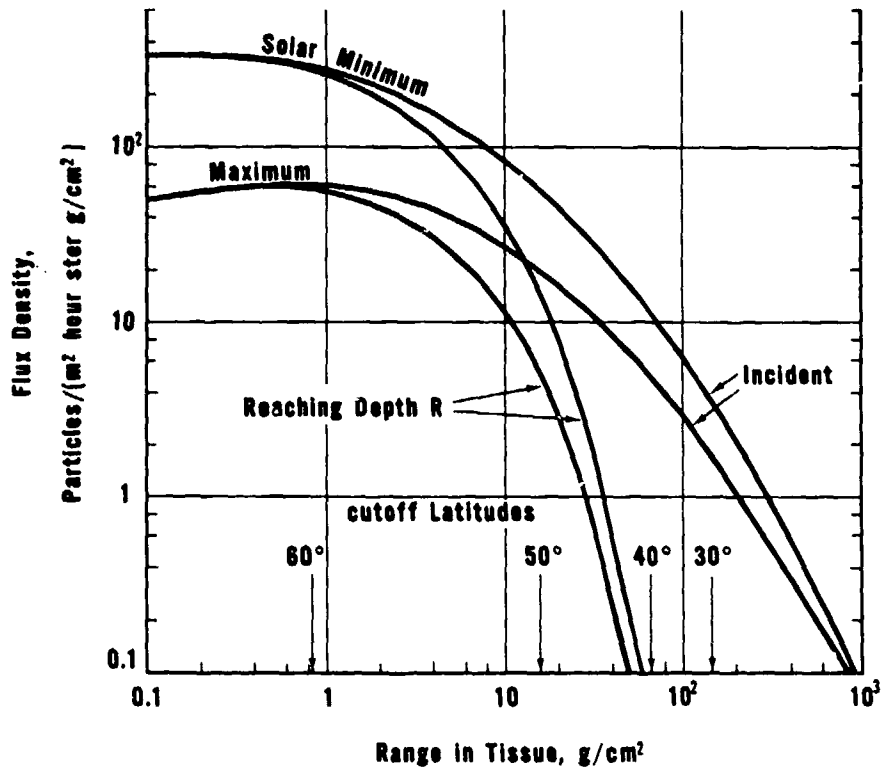
**ENERGY SPECTRA OF GALACTIC ALPHA PARTICLES
AT SOLAR MINIMUM AND MAXIMUM**

FIGURE 5



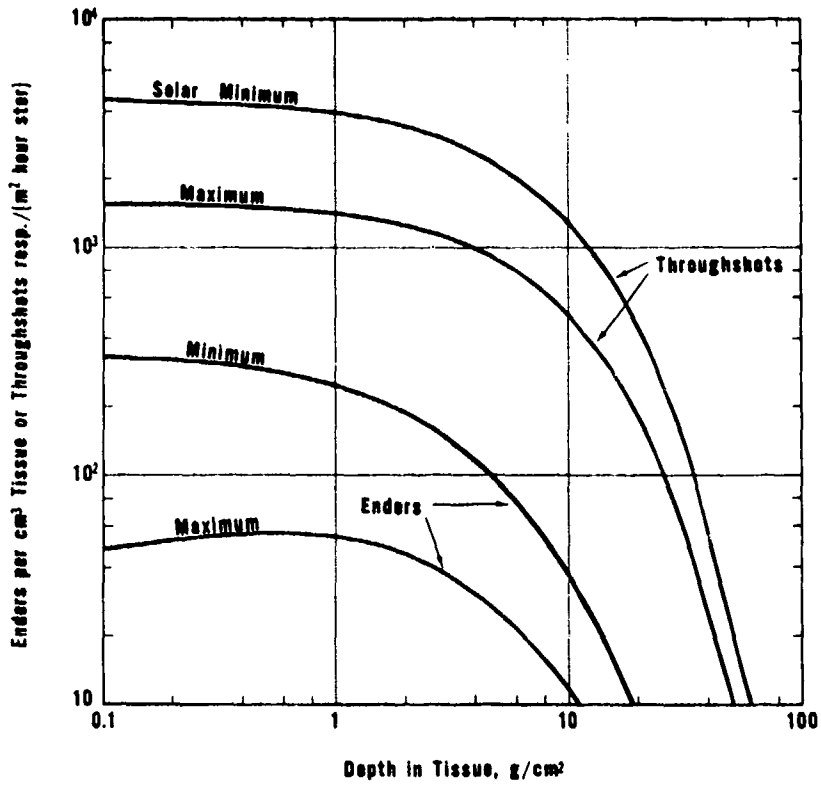
**DIFFERENTIAL RANGE SPECTRA OF GALACTIC ALPHA PARTICLES
AT SOLAR MINIMUM AND MAXIMUM**

FIGURE 6



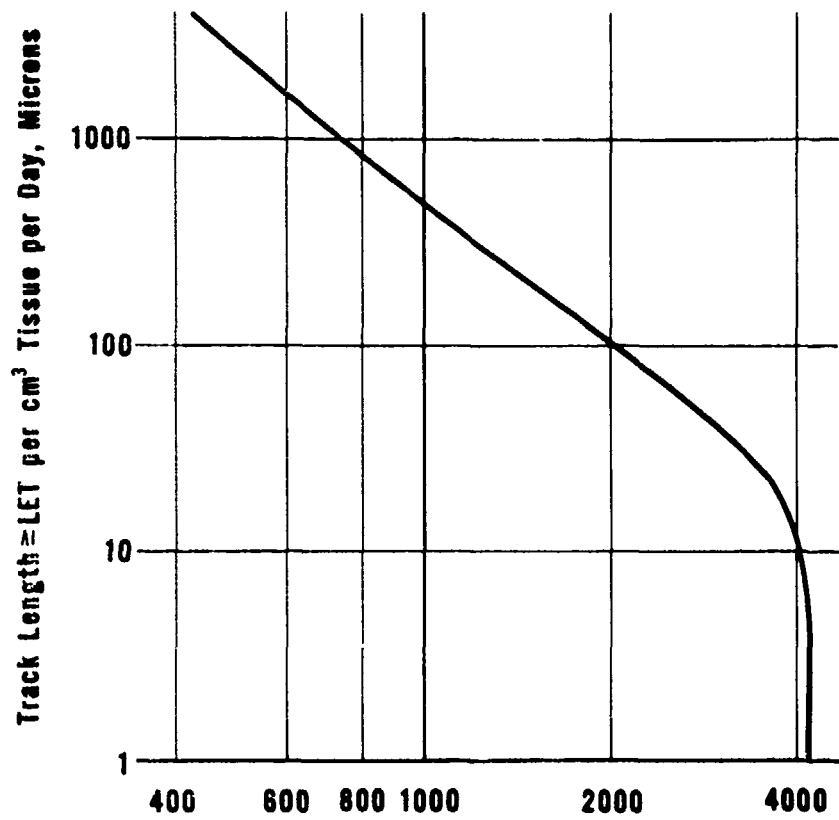
DIFFERENTIAL RANGE SPECTRA OF IRON GROUP (Z=24-28) AT SOLAR MINIMUM AND MAXIMUM

FIGURE 7



TRANSITION OF PARTICLES OF IRON GROUP IN TISSUE

FIGURE 8



LET, kev/micron Tissue
**INTEGRAL TRACK LENGTH DISTRIBUTION
 FOR IRON GROUP AT SOLAR MINIMUM**

FIGURE 9